Energy resolution and throughput of a new real time digital pulse processing system for x-ray and gamma ray semiconductor detectors

2013 JINST 8 P07019

(http://iopscience.iop.org/1748-0221/8/07/P07019)

PUBLISHED BY IOP PUBLISHING FOR SISSA MEDIALAB

RECEIVED: *March 22, 2013*
REVISED: *May 21, 2013*
ACCEPTED: *June 11, 2013*
PUBLISHED: *July 29, 2013*

Energy resolution and throughput of a new real time digital pulse processing system for x-ray and gamma ray semiconductor detectors

L. Abbene,[a,1] **G. Gerardi,**[a] **G. Raso,**[a] **S. Basile,**[b] **M. Brai**[a] **and F. Principato**[a]

[a] *Dipartimento di Fisica e Chimica,*
Viale delle Scienze, Edificio 18, 90128 Palermo, Italy
[b] *Dipartimento di Energia, Ingegneria dell'Informazione e Modelli Matematici,*
Viale delle Scienze, Edificio 6, 90128 Palermo, Italy

E-mail: abbene@unipa.it

ABSTRACT: New generation spectroscopy systems have advanced towards digital pulse processing (DPP) approaches. DPP systems, based on direct digitizing and processing of detector signals, have recently been favoured over analog pulse processing electronics, ensuring higher flexibility, stability, lower dead time, higher throughput and better spectroscopic performance. In this work, we present the performance of a new real time DPP system for X-ray and gamma ray semiconductor detectors. The system is based on a commercial digitizer equipped with a custom DPP firmware, developed by our group, for on-line pulse shape and height analysis. X-ray and gamma ray spectra measurements with cadmium telluride (CdTe) and germanium (Ge) detectors, coupled to resistive-feedback preamplifiers, highlight the excellent performance of the system both at low and high rate environments (up to 800 kcps). A comparison with a conventional analog electronics showed the better high-rate capabilities of the digital approach, in terms of energy resolution and throughput. These results make the proposed DPP system a very attractive tool for both laboratory research and for the development of advanced detection systems for high-rate-resolution spectroscopic imaging, recently proposed in diagnostic medicine, industrial imaging and security screening.

KEYWORDS: Digital signal processing (DSP); X-ray detectors

[1] Corresponding author.

doi:10.1088/1748-0221/8/07/P07019

Contents

2013 JINST 8 P07019

1 Introduction

The goal of X-ray and gamma ray spectroscopy system is to give accurate and precise measurement of input photon counting rate (ICR) and photon energy. Good and reliable spectroscopy systems should be able to provide true ICR, good energy resolution and small peak position shifts in the measured spectra over the widest range of ICRs. At modest ICRs, i.e. below a few tens of kcps, obtaining precise and accurate results from a conventional spectroscopic system is a relatively routine task. At higher ICRs, several problems like count losses, degradation of resolution and peak position shifts, start to appear.

Due to the increasing X-ray and gamma ray applications like synchrotron light experiments [1, 2], non-destructive X-ray inspection of objects [3] and the new energy-selective imaging techniques in diagnostic X-ray medicine (mammography, computed tomography) [4, 5], new spectroscopic systems with high-rate-resolution capabilities are required. Concerning the medical applications, typical diagnostic X-ray beams are characterized by photon fluence rates higher than 10^6 photons mm^{-2} s^{-1} and, in this hard environment, the development of high performance systems is still a great challenge. Beside the energy resolution, the system throughput, typically referred as the output counting rate (OCR) related to the ICR, is also a key parameter. Indeed, under specific experimental conditions in which the acquisition time is limited, high throughput is needed to obtain energy spectra with a good statistical confidence.

Each component, from the radiation detector to the pulse processing electronics, directly affects the performance of a spectroscopic system. Beside the properties of radiation detectors and

preamplifiers, the characteristics of the pulse processing electronics are also crucial in the development of high-rate performance spectrometers. Traditional pulse processing electronics consists of analog shaping amplifiers coupled to multichannel analyzers (MCAs): the detector signals (preamplifier output signals) are shaped and filtered by the shaping amplifier and finally processed by the MCA. The MCA evaluates and digitizes (by analog-to-digital converters) the height of the shaping amplifier output pulses and generates the pulse height histogram (energy spectrum). By selecting the proper shaping time constant of the amplifier, each system is well optimized either for good resolution (long shaping time constant) or for high throughput (short shaping time constant). At high ICRs, pulse pile-up (tail and peak pile-up [6]) and dead time losses are the major drawbacks and, despite the implementation of sophisticated baseline restoration and pile-up rejection techniques, analog pulse processing electronics fails in these hostile environments.

Recently, the high performance of the analog-to-digital converters (ADCs) has driven physicists and engineers to realize electronics in which the analog-to-digital conversion is performed as close as possible to the detector. Several groups [7–10] have proposed hybrid (i.e. both analog and digital) pulse processing chains, in which the shaped pulses from an analog amplifier are sampled by a digitizer (with sampling frequencies > 10 MHz) thus eliminating the dead time of MCAs. The digitized shaped pulses are processed off-line for pulse height analysis and pile-up inspections. These systems showed good spectroscopic performance up to photon counting rates of about 100 kcps, a limit due to the finite width of the shaped pulses and to the difficulties on baseline restoration. At higher counting rates, the direct digitization of the preamplifier output pulses (digital pulse processing approach) is a very appealing solution, as reported in several works [11–21]. In a digital pulse processing (DPP) system, the preamplifier output (CSP) signals are directly digitized by ADCs (with sampling frequencies $\geqslant 100$ MHz) and then processed by using digital algorithms. A DPP system leads to better results than the analog one, in terms of parameters such as stability, flexibility, reproducibility, energy resolution, throughput, dead time modelling and the possibility of shape preservation of the pulses for further analysis. In a DPP system, the direct digitizing of the detector signals minimizes the drift and instability normally associated with analog pulse processing. Once digitized, the pulses are immune to distortions caused by electronic noise and temperature instabilities. Moreover, it is possible to use complex algorithms for adaptive processing and optimum filtering, not easily implementable in a traditional analog approach. A DPP analysis also requires considerably less overall processing time than the analog ones ensuring lower dead time and higher throughput. In a DPP system there is no additional dead time associated with digitizing the pulses and so there is no MCA dead time (conversion time and data storage time). Preservation of the detector pulse shape for pulse shape analysis is also very important for performance enhancements [16, 18, 20], photon tracking [22] or particle identification [23].

Some DPP systems are composed by a digitizer and a personal computer for data recording and analysis (off-line analysis) [7–10, 14, 16–20]. Real time data processing [11–13, 21], in which the signals are acquired, recorded and processed on-line, is obtained by using digitizers with local memory and field programmable gate arrays (FPGA), wherein pulse processing algorithms can be implemented (DPP firmware).

In this work, we report on the performance of a new real time DPP system for X-ray and gamma ray semiconductor detectors. The system is based on a modified version of a commercial digitizer equipped with a custom DPP firmware, developed by our group, for on-line pulse shape

2013 JINST 8 P07019

and height analysis. Experimental results on cadmium telluride (CdTe) and germanium (Ge) detectors, at both low and high photon counting rates, are reported. Moreover, a parallel comparison with a standard analog pulse processing electronics, in terms of energy resolution and throughput, is also performed.

2 Detectors and operation

To investigate on the performance of the DPP system, we used two different semiconductor detectors: a thin planar CdTe detector and a coaxial Ge detector (p-type). As well known, thin CdTe/CdZnTe detectors (1–2 mm thick) are very appealing for X-ray spectroscopy in the 1–100 keV energy range [24]–[32], while coaxial p-type Ge detectors are excellent spectrometers in the gamma energy range ($>$ 100 keV) [6, 26, 33]. We used a planar CdTe detector (XR100T-CdTe, S/N 6012, Amptek, U.S.A.) with a thickness of 1 mm (absolute efficiency of 64% at 100 keV) [16] and a coaxial Ge detector (GEM40P4-76, Ortec, U.S.A.) with a crystal diameter of 64.1 mm and a crystal length of 64.4 mm (relative efficiency of 40% at 1.33 MeV) [34]. Both detectors are equipped with resistive-feedback charge sensitive preamplifiers (CSPs).

For comparison, a standard analog pulse processing chain was also used. The preamplifier output pulses were shaped by an analog shaping amplifier (672, Ortec, U.S.A.), equipped with different shaping time constant values of 0.5, 1, 2, 3, 6 and 10 μs. The semi-Gaussian output pulses were acquired by a standard multichannel analyzer (MCA-8000A, Amptek, U.S.A.).

We measured the system response to four X-ray and gamma ray calibration sources (^{109}Cd: 22.1, 24.9 and 88.1 keV; ^{241}Am: 59.5 keV; ^{137}Cs: 661.7 keV; ^{60}Co: 1173.2 keV and 1332.5 keV). To obtain different impinging photon counting rates, we changed the irradiated area of the detectors using collimators (Pb and W) with different geometries.

3 DPP system

The digital system is composed by a digitizer and a PC, where the user can set the DPP parameters, choose the working mode and display the results by using a Labview program, developed by our group (Control and Display software). Figure 1 shows a picture and the block diagram of the digital system coupled to the CdTe detector.

The pulse processing analysis is performed by using a custom DPP firmware, developed by our group and uploaded to the digitizer. To digitize the preamplifier output waveform, we used a commercial digitizer (DT5724, CAEN S.p.A., Italy), housing high speed ADCs (14 bit and 100 MS/s), a buffer memory and ALTERA Cyclone EP1C20 FPGAs. The digitizer is equipped with 4 channels (*AC* coupled). Each channel is characterized by one ADC with three full scale ranges ($\pm$1.125 V, $\pm$0.5625 V and $\pm$0.2813 V). The data stream from each ADC is written in four circular memories without dead time. The digital pulse processing is carried out by the dedicated FPGA, in which the DPP method is implemented (DPP firmware). The produced data are packed and another FPGA collects and sends them, via USB channel, to the PC.

3.1 DPP firmware

The DPP firmware is based on a revised version of a DPP method, developed by our group and successfully used for off-line analysis [14, 16–19]. The pulse detection is performed by using a

2013 JINST 8 P07019

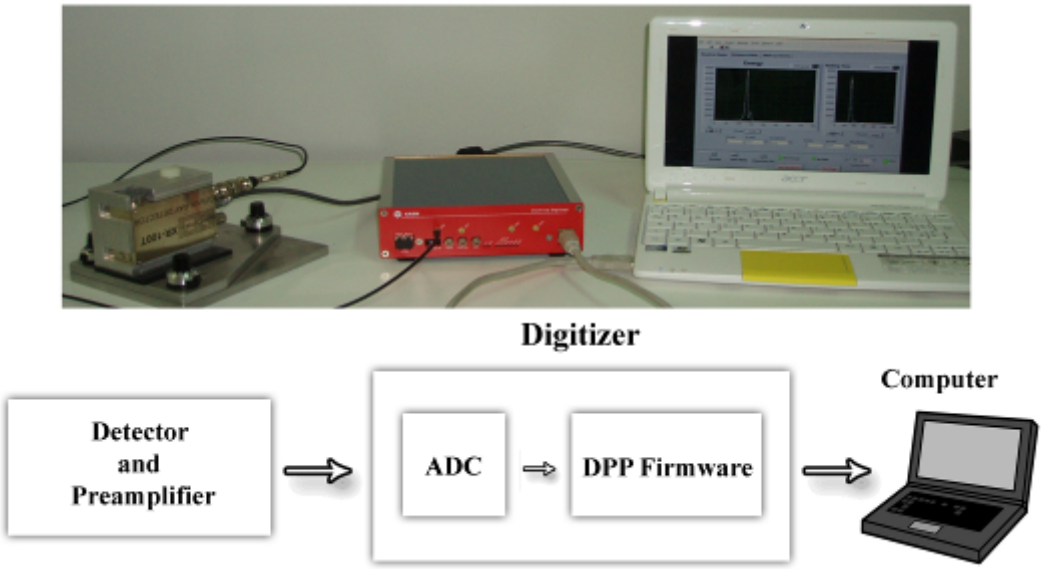

Figure 1. The digital system coupled to the CdTe detector.

"*fast*" shaping mode, while the pulse shape and height analysis (PSHA) starts with a "*slow*" shaping mode.

The DPP firmware is characterized by two main features: (i) it performs the PSHA of each event on single isolated input waveform windows to avoid the corruptions that the analysis can produce to adjacent pulses and (ii) due to an automatic baseline restoration (based on the analysis on single pulses), it also allows *AC* coupling. This approach allows the elimination of the average value of the preamplifier output waveform and so the maximum exploitation of the ADC input ranges.

In the following subsections, we summarize the main operations performed by the DPP firmware.

3.1.1 Pulse detection: *fast shaping mode*

Once digitized, the preamplifier output waveform is shaped by using the classical single delay line (SDL) shaping technique [6]. Shaped pulses are obtained by subtracting from the original waveform its short delayed and attenuated fraction. The attenuation is able to avoid undesirable undershoots in the shaped pulses, therefore, working as the classical pole-zero cancellation technique [6]. The width of each shaped pulse (*fast SDL pulses*) is equal to $T_d + T_p$, wherein $T_d$is the delay time and T_p is the peaking time of the original pulse. This shaping operation (*fast shaping mode*), characterized by a short delay time, is able to detect the pulses (i.e. the events) from the preamplifier output waveform with high time resolution, as shown in figure 2. A *trigger* signal is generated and time tagged when the falling edge of the shaped pulses crosses a height threshold.

Because the width of each shaped pulse is well known, it is possible to perform a pile-up inspection within the fast shaping operation (*fast pile-up rejection*). If the width of a shaped pulse exceeds a maximum width threshold (ΔT_{fast}), the pulse is classified as representative of a peak pile-up event and rejected for the pulse height analysis.

2013 JINST 8 P07019

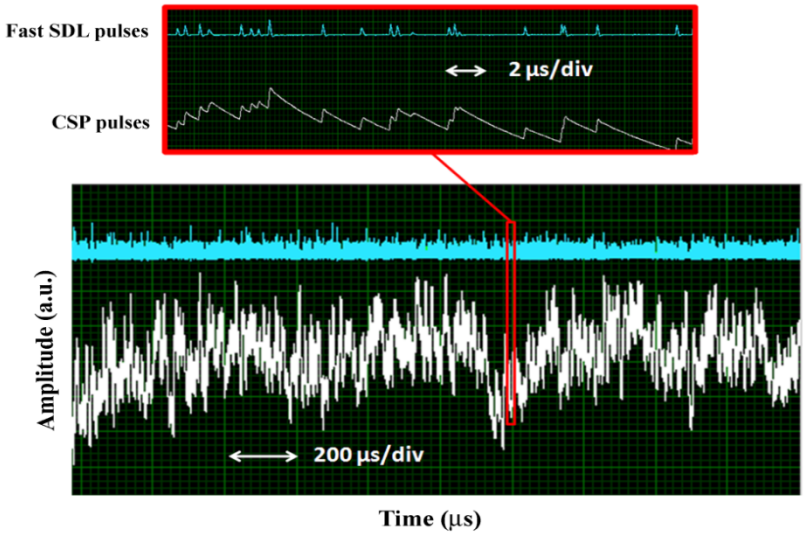

Figure 2. The digitized preamplifier output (CSP) pulses (white line) and the shaped pulses (cyan line) through the fast shaping operation. A zoom of the picture clearly shows the good detection of the pulses from the waveform. The pulses represent ^{241}Am photons impinging on the CdTe detector with a ICR of 825 kcps.

3.1.2 Pulse Shape and Height Analysis (PSHA): *slow shaping mode*

First, the DPP method performs a further pile-up inspection (*slow pile-up rejection*). The trigger signal will detect a not piled up event if there are not other triggers within a selected time window (centered on the trigger signal) of the preamplifier output waveform. The width of the window is termed *snapshot time* (ST) and all the not piled up events are analyzed. In order to avoid the corruptions that the analysis can produce to adjacent pulses, the DPP method performs the PSHA of the selected events on the extracted *snapshot* waveform, ST wide, centered on the trigger. Figure 3 shows three snapshot waveforms, with each maximum amplitude at the center position of the window ($ST = 3\,\mu$s), at different ICRs. It is clearly visible that the waveform decay, before and after the leading edge of each pulse, depends on the ICR. This effect is due to the piling up of the pulses on the exponential tail of previous pulses, that rises up as the ICR increases.

Once extracted, the snapshot waveform is shaped by using a slow SDL operation, characterized by a longer delay time than the fast one (we used a delay time $= ST/4$). The slow SDL shaping is used to perform: (i) a baseline restoration, by evaluating the mean value of the samples preceding the leading edge of the shaped pulses, (ii) a pulse shape analysis, by evaluating the maximum amplitude and the rise time of the shaped pulses and (iii) the height analysis of the shaped pulses. By using the proper decay constant value, the slow SDL shaping allows elimination of the influence of the previous events on each selected pulse and, through the baseline recovery, the minimization of baseline shifts (due to *AC* coupling and *DC* offsets), that are more severe at high ICRs. The maximum amplitude of the shaped pulses is obtained after compensation of the exponential decay by using a digital deconvolver [35]. The shape analysis consists in the measurement of the peaking

2013 JINST 8 P07019

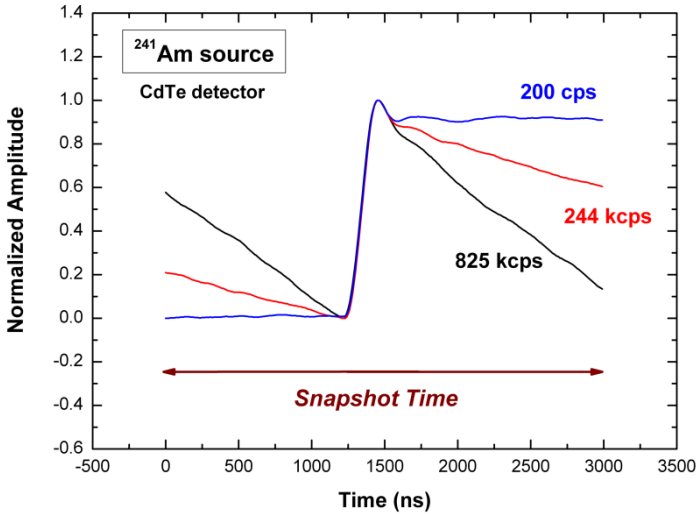

Figure 3. Single isolated preamplifier output pulses, within a snapshot time $ST = 3\,\mu$s, at different ICRs. The waveform decay changes, before and after the leading edge of each pulse, are due to the different number of piled up pulses. The pulses represent ^{241}Am photons impinging on the CdTe detector. Each pulse is arbitrary vertically shifted and normalized to its maximum amplitude.

time of the shaped pulses. The rise time of the pulses, i.e. the interval between the times at which the shaped pulse reaches 10% and 90% of its maximum amplitude, is first evaluated. The times, corresponding to the exact fractions (10% and 90%) of the pulse height, are obtained through a linear interpolation. The method estimates the peaking time equal to 2.27 times the rise time (i.e. about five times the time constant) with a precision of 2 ns.

Finally, the pulse height (event energy) estimation is performed by applying an optimized low-pass filter to all the samples of each the shaped and deconvolved pulse.

As well known [6, 16–19], the correlation between the height and the peaking time of the pulses can be generally used to minimize both incomplete charge collection and peak pile-up effects. In this work, we used this correlation to minimize peak pile-up effects (i.e. overlapped preamplifier output pulses within the peaking time that are not detected through the fast shaping operation) in the measured spectra. Because, the peak pile-up pulses are characterized by a longer peaking time and a higher height than the correct pulses, it is possible to reduce their effects in the measured spectra by analyzing both the peaking time and the height (energy) distribution of the pulses [16–19]. We implemented a pulse shape discrimination (PSD) technique based on the selection of the proper peaking time region.

3.1.3 Dead time correction

The well defined dead time modelling is one of the most interesting characteristics of our DPP system. Knowledge of the dead time and of its analytic model is very important to estimate the true input counting rate. Both the maximum width threshold ΔT_{fast} and the snapshot time ST are dead times for the DPP system and they can be used in a paralyzable model [6].

For Poisson random processes, the paralyzable dead time τ, the true photon counting rate n and the measured photon counting rate m satisfy the following equation (see, for instance, [6], p. 123):

$$m = n\exp(-n\tau)\,. \tag{3.1}$$

2013 JINST 8 P07019

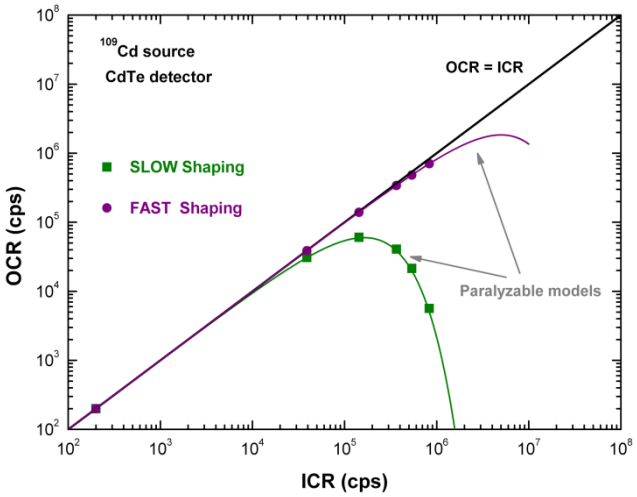

Figure 4. Throughput of the DPP system: the output photon counting rates (OCRs) from fast and slow shaping versus the true input counting rate (ICR). The purple and green lines are the paralyzable dead time model functions for the fast shaping (dead time of 200 ns) and with a ST of 6 μs. ICR was calculated through the equation (3.1), the knowledge of the dead time and by using the measured OCR from the fast shaping. The system processed the ^{109}Cd events measured with the CdTe detector.

It is possible to evaluate the true rate n from the measured rate m by iteratively solving the above equation. Nevertheless, the above equation can be solved exploiting the properties of the Lambert W function [36]. The Lambert $W(k,z)$ function is implicitly defined by the following equation:

$$W(k,z)\exp[W(k,z)] = z. \tag{3.2}$$

It has, in general, complex values even for real values of z, but has two real valued branches, namely for $k = 0, -1$. It is implemented in most commercially and freely available mathematical software.

The two solutions of eq. (3.1) corresponding to the same value of m can then be found as:

$$n_1 = -\frac{W(0,-m\tau)}{\tau} \tag{3.3}$$

and

$$n_2 = -\frac{W(-1,-m\tau)}{\tau} \tag{3.4}$$

for n smaller and larger than τ^1, respectively.

In the fast shaping mode, the true rate is always smaller than τ_f^{-1} (with $\tau_f = \Delta T_{\text{fast}} = 200$ ns), therefore it can be calculated through the W function with $k = 0$. The calculated value can then be associated with the corresponding measured rates in the slow shaping mode. As a double check, the true rates for the slow shaping mode have been calculated using the W functions with both $k = 0$ and -1, in order to determine the true rates for values smaller or larger than τ_s^{-1}(with $\tau_s = ST = 6\,\mu$s). The two procedures have shown a very good numerical agreement.

Therefore, the DPP system is then always able to estimate the true rate through the equation (3.1), the knowledge of the dead time and by using the measured OCR. Figure 4 shows the rate of the events analyzed by the fast shaping ($\Delta T_{\text{fast}} = 200$ ns) and with a $ST = 6\,\mu$s versus the true input counting rate (^{109}Cd events measured by using the CdTe detector).

2013 JINST 8 P07019

As shown in figure 4, the measured rates from both the fast and the slow shaping are in agreement with the paralyzable dead time model. This result highlights as our DPP system is always able to estimate the true rate of the impinging photons through the fast channel, even for low rates in the spectrum (slow channel). Therefore, it is possible to use long *ST* values (low throughput) for optimum pulse height analysis (optimum energy resolution) without perturbing the correct estimation of the input photon counting rate.

3.1.4 Working modes

To obtain the overall features of the impinging photons, the DPP can transmit one of the following several results to PC: (i) input waveform, (ii) fast shaping waveform, (iii) energy and peaking time list, (iv) energy, peaking time and time of occurrence list, (v) time of occurrence and reshaped (after base line restorer and exponential time decay correction) pulse leading edge list and (vi) the snapshot waveform (a sequence of preamplified pulses with their time of occurrence). In the last working mode, the system only transmits the preamplified pulses selected for the pulse height analysis, i.e. not piled-up with the preceding and following pulses in the input waveform. Each pulse is presented within a time window equal to the selected snapshot time. Contrary to what happens in analog pulse processing systems or in other DPPs using similar processing operations, the preamplifier pulse shape is preserved. We stress that each data, packed as required from the selected working mode, is coupled to the following housekeeping data: time stamp of the packed data, total accumulated dead time, number of fast detected pulse, number of analysed events, number of pile-up events (slow and fast pile-up rejection). From this data the user can derive, with high time resolution, the related count rates. Each working mode is set through the control and display software.

4 Measurements and results

In the following sections, we will show the performance of the DPP system, in terms of energy resolution and throughput, coupled to CdTe and Ge detectors. Comparisons with the analog electronics will be also highlighted.

4.1 X-ray spectroscopy with a CdTe detector

We measured X-ray spectra at low and high ICRs by using both the analog and the DPP systems. At low ICR (200 cps), the DPP system shows similar performance to the analog one. On the contrary, important differences between the two approaches were well highlighted at high ICRs. We investigated on the high-rate performance of the DPP system by analyzing the stability of both peak position (centroid) and energy resolution at various ICRs. We measured ^{109}Cd and ^{241}Am spectra at various ICRs with both systems working at similar throughput. Concerning the analog electronics, we used a shaping time constant of 0.5 μs (the smallest selectable value from the analog amplifier) that is the best value for both maximum throughput and optimum energy resolution at ICRs $>$ 30 kcps (this result was obtained experimentally by analyzing ^{109}Cd and ^{241}Am spectra at different shaping time constant values and at different ICRs). To obtain a similar analog throughput, we used a *ST* of 3.4 μs and 4.2 μs for ^{109}Cd and ^{241}Am sources, respectively. The measurements are shown in figure 5.

2013 JINST 8 P07019

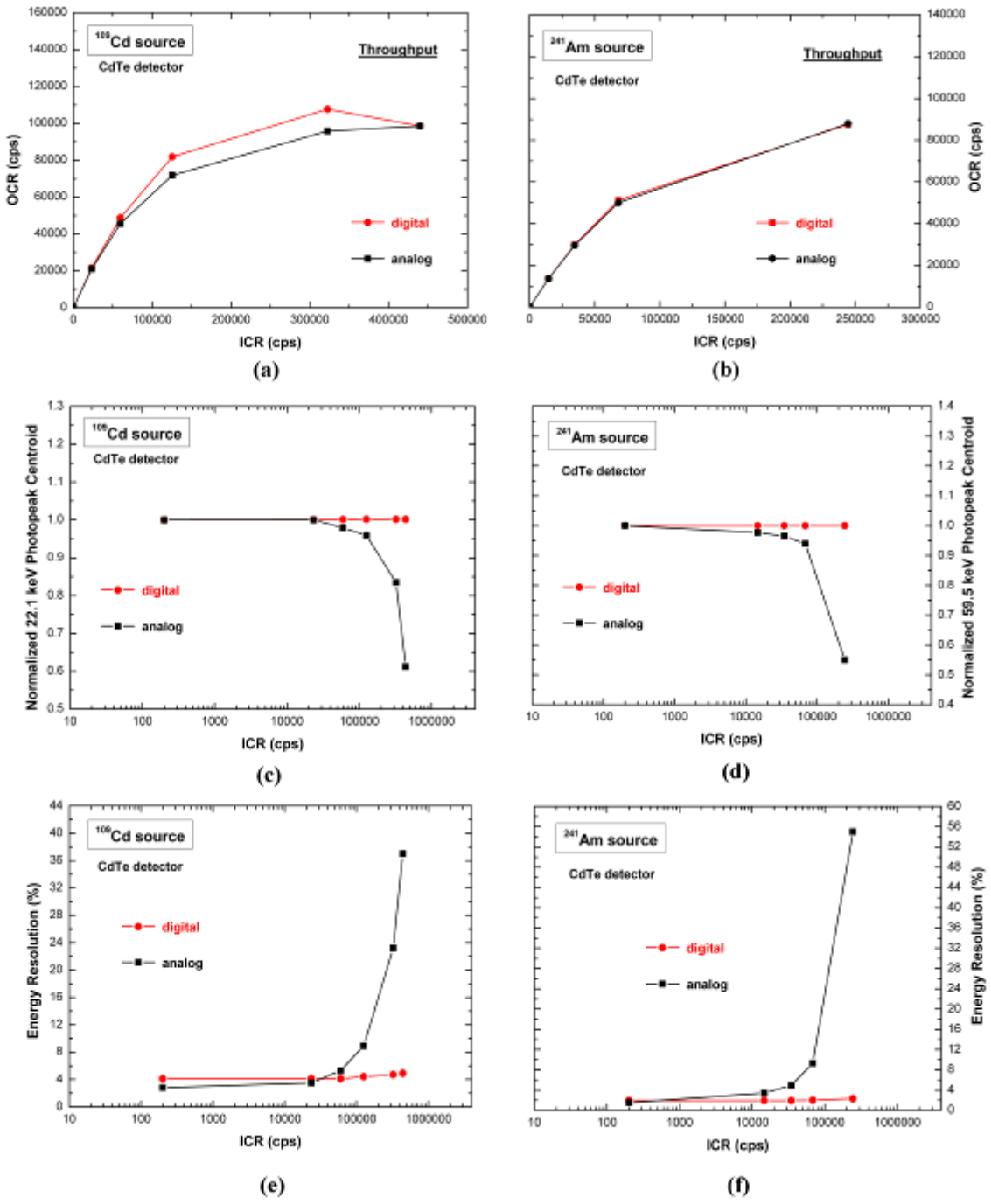

Figure 5. Performance comparison of the DPP system and the analog pulse processing electronics at various ICRs; both systems are characterized by similar throughput (OCR vs. ICR curve). Throughput of both systems: a) ^{109}Cd and b) ^{241}Am sources. Normalized c) 22.1 keV and d) 59.5 keV photopeak centroids vs. ICR. Energy resolution at e) 22.1 keV and f) 59.5 keV vs. ICR.

2013 JINST 8 P07019

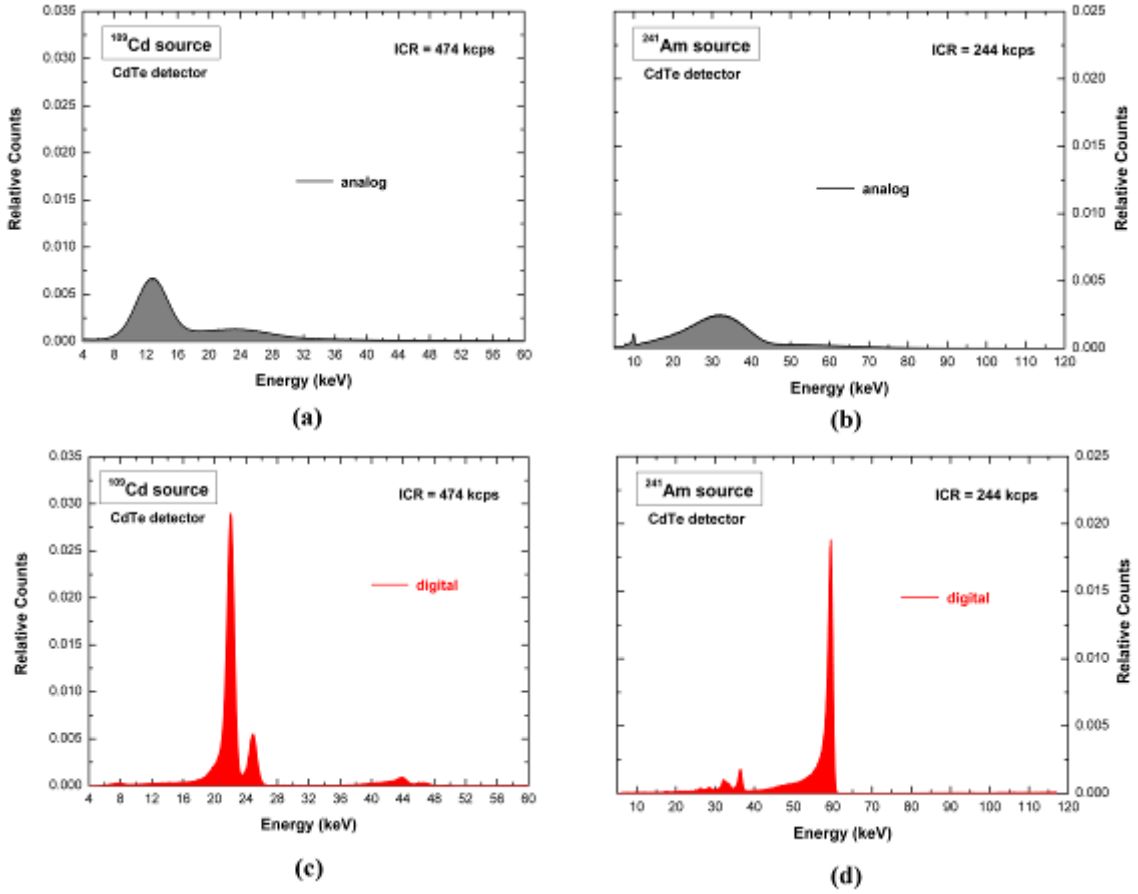

Figure 6. ^{109}Cd and ^{241}Am spectra measured with the CdTe detector by using the analog (shaping time constant value of 0.5 μs) and the DPP system (*ST* of 3.4 μs and 4.2 μs for ^{109}Cd and ^{241}Am sources, respectively). (a), (b) The high peak shift and the high energy resolution degradation highlight the limits of the analog system in compensating the baseline shifts and pile-up effects, that are more severe at high ICRs. (c), (d) These results highlight the good high rate capability of the DPP system. The counts were normalized to the total number of the detected events. Energy calibration was performed at low ICR.

The maximum rate range is fixed by the limits of the analog pulse processing electronics (analog amplifier). The results clearly highlight the limits of the analog chain at high ICRs. The ^{109}Cd spectra measured with the analog chain are characterized by a peak centroid shift equal to 39% at 474 kcps (45% for ^{241}Am spectra at 244 kcps) and by high resolution degradation. These distortions are due to baseline shifts and pile-up effects that are more severe at high ICRs. On the contrary, the spectra acquired by the DPP chain are characterized by no peak position shifts and better energy resolution: 4.9% FWHM at 22.1 keV at 474 kcps (analog: 37%) and 2.3% FWHM at 59.5 keV at 244 kcps (analog: 55%). Figure 6 shows the high-rate spectra measured with both systems.

To better highlight the potentialities of the DPP system or for high throughput or for optimum energy resolution, we performed measurements at various OCRs. Figure 7 shows the measured energy resolution vs. throughput (i.e. OCR/ICR) for some ICR conditions. The different throughput conditions are obtained by varying only the *ST* of the DPP system. In this last analysis, the maxi-

2013 JINST 8 P07019

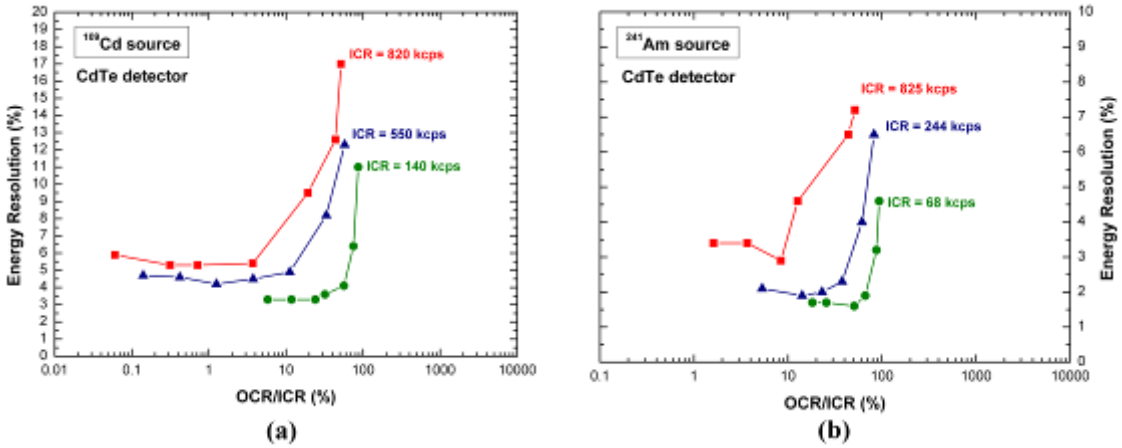

Figure 7. Energy resolution vs. throughput (i.e. OCR/ICR) for some ICR conditions. The energy spectra were measured with the CdTe detector and by using the DPP system. The different throughput conditions are obtained by varying the *ST* of the DPP system.

mum rate range is fixed by the limits of the preamplifier (i.e. saturations occur at higher ICRs due to its energy rate limit). Energy spectra at low and high throughput are shown in figure 8. We also used the pulse shape discrimination (PSD) to minimize peak pile-up events in the measured spectra.

4.2 Gamma-ray spectroscopy with a Ge detector

^{137}Cs and ^{60}Co spectra were measured with the Ge detector at both low and high ICRs. Figure 9 shows the spectra measured with the DPP system at low ICRs. We used a *ST* of 25 μs and 30 μs for ^{137}Cs and ^{60}Co spectra, respectively. Energy resolutions (0.29% FWHM at 662 keV and 0.17% at 1333 keV) are similar to the values measured with the analog electronics (0.32% FWHM at 662 keV and 0.18% at 1333 keV, by using a shaping time constant value of 6 μs).

We also measured ^{137}Cs spectra at various ICRs (up to 55 kcps) with both analog and DPP systems, working at similar throughput (inset of figure 10a). To obtain a similar analog throughput, we used a *ST* of 25 μs (DPP) and a shaping time constant of 6 μs (analog). Figure 10 shows the energy resolution at various ICRs (figure 10a) and energy resolution vs. throughput at 55 kcps (figure 10b). ^{137}Cs spectra measured with both systems at low and high throughput are shown in figures 11 and 12.

2013 JINST 8 P07019

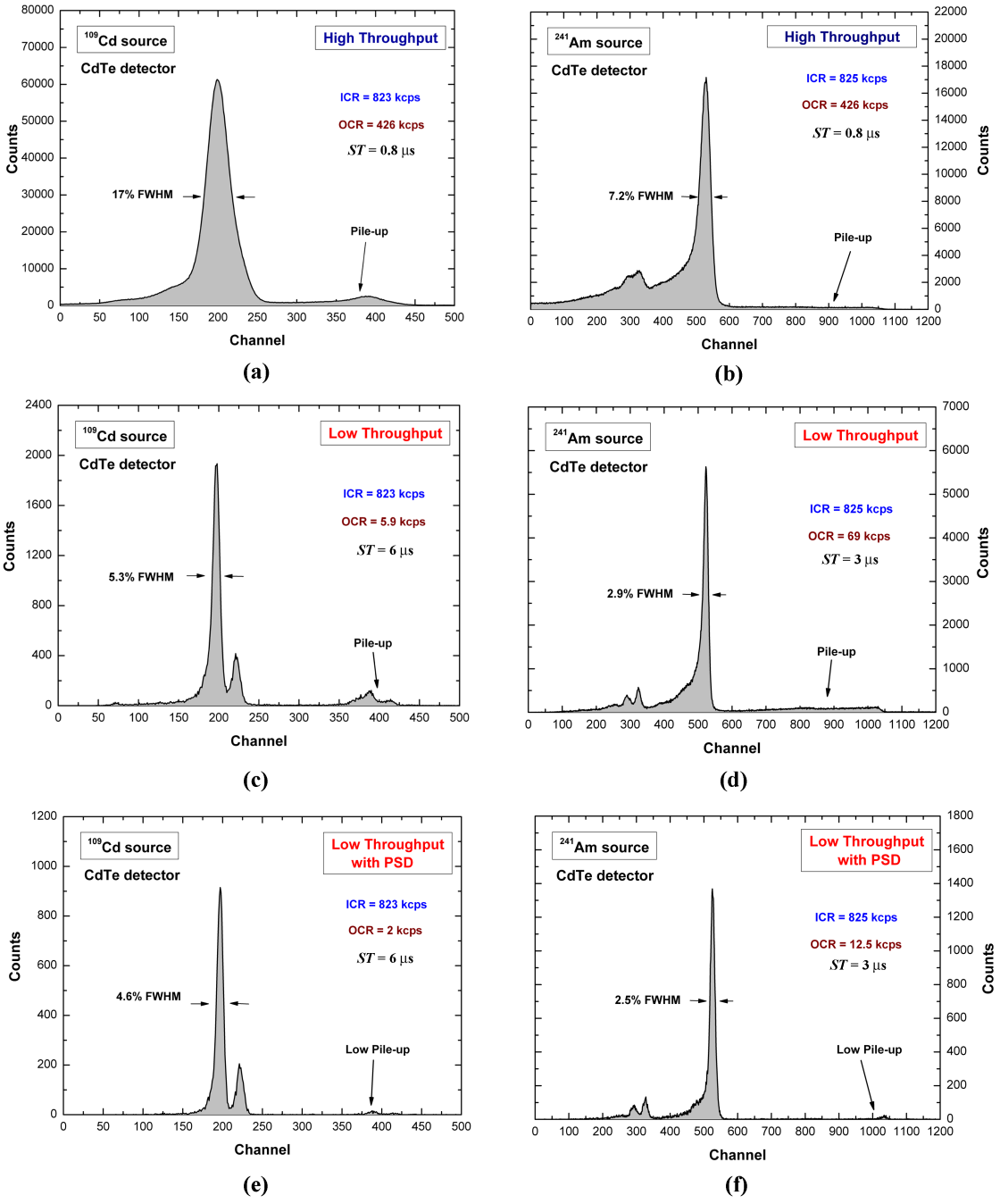

Figure 8. ^{109}Cd and ^{241}Am spectra measured with the CdTe detector. The spectra show the performance of the DPP system at high and low throughput. The different throughput conditions are obtained by varying the *ST* of the DPP system. Pulse shape discrimination (PSD) technique was also used to reduce peak pile-up (e) and (f).

2013 JINST 8 P07019

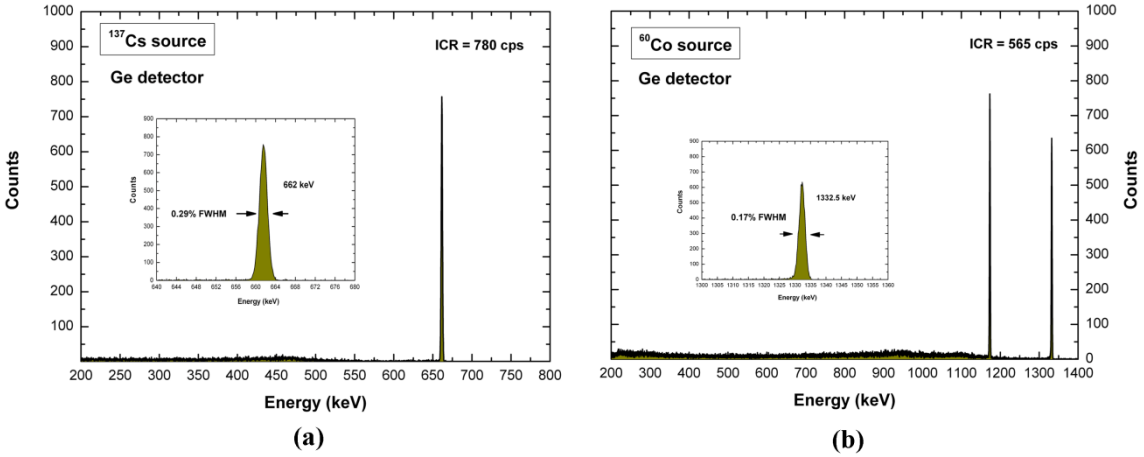

Figure 9. ^{137}Cs and ^{60}Co spectra measured with the Ge detector and the DPP system. Spectra exhibit energy resolution of 0.29% FWHM at 662 keV and 0.17% at 1333 keV.

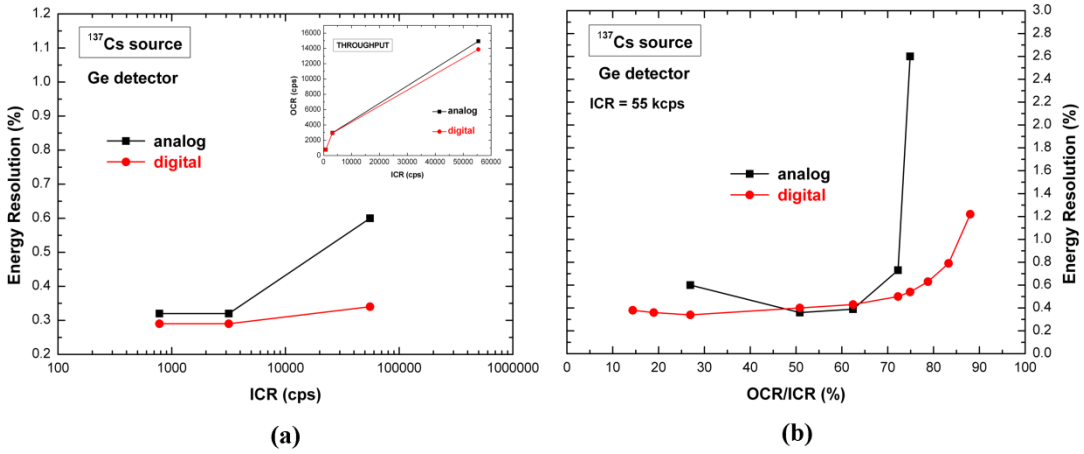

Figure 10. (a) Energy resolution at 662 keV vs. ICR, measured with both the DPP and the analog systems working at similar throughput. (b) Energy resolution vs. throughput at 55 kcps. The different throughput conditions are obtained by varying the *ST* of the DPP system and the shaping time constant of the analog amplifier.

2013 JINST 8 P07019

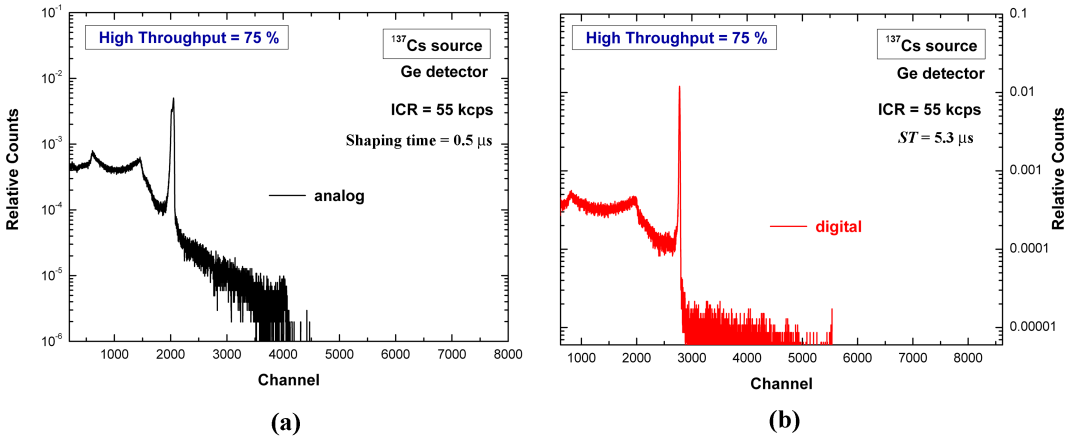

Figure 11. ^{137}Cs spectra measured at high throughput (75 %) with (a) analog and (b) DPP systems. (a) Energy resolution of 2.6 % FWHM at 662 keV; (b) energy resolution of 0.5 % FWHM at 662 keV.

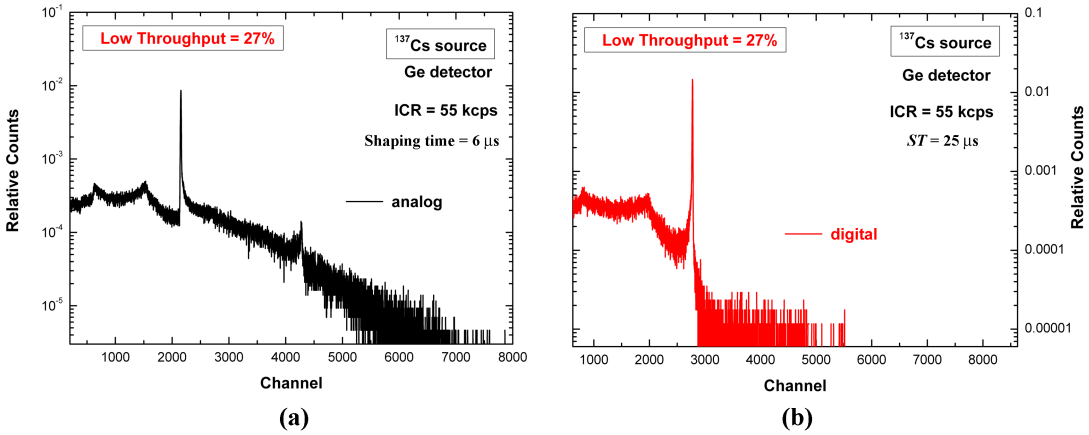

Figure 12. ^{137}Cs spectra measured at low throughput (27 %) with (a) analog and (b) DPP systems. Energy resolution of 0.6 % FWHM at 662 keV; (b) energy resolution of 0.3 % FWHM at 662 keV.

5 Conclusions

A new digital pulse processing (DPP) system for X-ray and gamma ray semiconductor detectors was presented. The system, based on a commercial digitizer equipped with a custom DPP firmware, developed by our group, is able to perform on-line pulse height and shape analysis. Through the setting of various working modes, the system is able to perform a full characterization of impinging radiation (true rate, time of occurrence, energy, interaction position). The system, characterized by a well defined dead time model (paralyzable), is able to perform an accurate estimation of the true photon counting rates. Low-rate measurements of X-ray and gamma ray spectra with CdTe and Ge detectors highlighted the good spectroscopic performance of the DPP system, in agreement with conventional analog pulse processing systems. Excellent results were obtained at high rates (up to rate limit of preamplifer): (i) low degradation of energy resolution, (ii) good stability of peak position, (iii) high throughput and (iv) minimization of peak pile-up through pulse shape

2013 JINST 8 P07019

analysis. Moreover, a comparison with a conventional analog electronics showed the better high-rate-resolution capabilities of the digital approach.

We stress an important feature of our DPP system: *once the parameters are set for the particular detector, no further settings are required when the input rates are changed, contrary to what happens by using conventional pulse processing systems*.

The DPP system is a very attractive tool for both laboratory research and for the development of advanced energy resolved photon counting detectors, recently proposed in diagnostic medicine (computed tomography and mammography), industrial imaging and security screening [37–41].

References

[1] V. Radicci et al., *EIGER a new single photon counting detector for X-ray applications: Performance of the chip*, 2012 *JINST* **7** C02019.

[2] A. Cecilia et al., *Investigation of crystallographic and detection properties of CdTe at the ANKA synchrotron light source*, 2011 *JINST* **6** P10016.

[3] P. Soukup et al., *X-ray color imaging with 3D sensitive voxel detector*, 2011 *JINST* **6** C12014.

[4] P.M. Shikhaliev et al., *Projection x-ray imaging with photon energy weighting: experimental evaluation with a prototype detector*, *Phys. Med. Biol.* **54** (2009) 4971.

[5] L.F.N.D. Carramate et al., *Energy weighting technique in Quantum Computed Tomography using a MPGD*, 2011 *JINST* **6** C02002.

[6] G.F. Knoll, *Radiation detection and measurements*, Fourth Edition, John Wiley and Sons, Inc., New York U.S.A. (2010).

[7] L. Abbene et al., *X-ray spectroscopy and dosimetry with a portable CdTe device*, *Nucl. Instrum. Meth.* **A 571** (2007) 373.

[8] U. Bottigli et al., *Comparison of two portable solid state detectors with an improved collimation and alignment device for mammographic x-ray spectroscopy*, *Med. Phys.* **33** (2006) 3469.

[9] S. Stumbo et al., *Direct analysis of molybdenum target generated x-ray spectra with a portable device*, *Med. Phys.* **31** (2004) 2763.

[10] A. La Manna et al., *Portable CdTe detection system for mammographic X-ray spectroscopy*, *Nuovo Cimento* **C 29** (2006) 361.

[11] M. Bolic and V. Drndarevic, *Digital gamma-ray spectroscopy based on FPGA technology* *Nucl. Instrum. Meth.* **A 482** (2002) 761.

[12] J.M. Cardoso et al., *CdZnTe Spectra Improvement through Digital Pulse Amplitude Correction using the Linear Sliding Method*, *Nucl. Instrum. Meth.* **A 522** (2004) 487.

[13] M. Arnold et al., *TNT digital pulse processor*, *IEEE Trans. Nucl. Sci.* **53** (2006) 723.

[14] G. Gerardi et al., *Digital filtering and analysis for a semiconductor X-ray detector data acquisition*, *Nucl. Instrum. Meth.* **A 571** (2007) 378.

[15] T. Papp and J.A. Maxwell, *A robust digital signal processor: Determining the true input rate*, *Nucl. Instrum. Meth.* **A 619** (2010) 89.

[16] L. Abbene et al., *Performance of a digital CdTe x-ray spectrometer in low and high counting rate environment*, *Nucl. Instrum. Meth.* **A 621** (2010) 447.

2013 JINST 8 P07019

[17] L. Abbene et al., *High-rate x-ray spectroscopy in mammography with a CdTe detector: a digital pulse processing approach*, *Med. Phys.* **37** (2010a) 6147.

[18] L. Abbene and G. Gerardi, *Performance enhancements of compound semiconductor radiation detectors using digital pulse processing techniques*, *Nucl. Instrum. Meth.* **A 654** (2011) 340.

[19] L. Abbene et al., *Direct measurement of mammographic X-Ray spectra with a digital CdTe detection system*, *Sensors* **12** (2012) 8390.

[20] M. Nakhostin and P. Veeramani, *A new method for charge-loss correction of room-temperature semiconductor detectors using digital trapezoidal pulse shaping*, 2012 *JINST* **7** P06006.

[21] L. Abbene, G. Gerardi and F. Principato, *Real time digital pulse processing for X-ray and gamma ray semiconductor detectors*, *Nucl. Instrum. Meth.* **A** (2013).

[22] K. Vetter et al., *Three-dimensional position sensitivity in two-dimensionally segmented HP-Ge detectors*, *Nucl. Instrum. Meth.* **A 452** (2000) 223.

[23] M. Mutterer et al., *Breakthrough in pulse-shape based particle identification with silicon detectors*, *IEEE Trans. Nucl. Sci.* **47** (2000) 756.

[24] S. Del Sordo et al., *Spectroscopic performances of* 16×16 *pixel CZT imaging hard-X-ray detectors*, *Nuovo Cimento* **B 119** (2004) 257.

[25] S. Del Sordo et al., *Characterization of a CZT focal plane small prototype for hard X-ray telescope*, *IEEE Trans. Nucl. Sci.* **52** (2005) 3091.

[26] S. Del Sordo et al., *Progress in the development of CdTe and CdZnTe semiconductor radiation detectors for astrophysical and medical applications*, *Sensors* **9** (2009) 3491.

[27] L. Abbene et al., *Spectroscopic response of a CdZnTe multiple electrode detector*, *Nucl. Instrum. Meth.* **A 583** (2007) 324.

[28] L. Abbene et al., *Hard x-ray response of pixellated CdZnTe detectors*, *J. Appl. Phys.* **105** (2009) 124508.

[29] N. Auricchio et al., *Charge transport properties in CdZnTe detectors grown by the vertical Bridgman technique*, *J. Appl. Phys.* **110** (2011) 124502.

[30] F. Principato et al., *Time-dependent current-voltage characteristics of Al/p-CdTe/Pt x-ray detectors*, *J. Appl. Phys.* **112** (2012) 094506.

[31] L. Abbene et al., *Experimental results from Al/p-CdTe/Pt X-ray detectors*, *Nucl. Instrum. Meth.* **A** (2013).

[32] F. Principato et al., *Polarization phenomena in Al/p-CdTe/Pt X-ray detectors*, *Nucl. Instrum. Meth.* **A** (2013).

[33] G.R. Gilmore, *Practical gamma-ray spectrometry*, John Willey and Sons, Inc., Chichester, West Sussex, U.K. (2008).

[34] Quality Assurance Data Sheet, GEM40P4-76, Ortec, U.S.A.

[35] V.T. Jordanov et al., *Digital techniques for real-time pulse shaping in radiation measurements*, *Nucl. Instrum. Meth.* **A 353** (1994) 261.

[36] R. Corless et al., *On the Lambert W function*, *Adv. Comput. Math.* **5** (1996) 329.

[37] J.S. Iwanczyk et al., *Photon counting energy dispersive detector arrays for X-ray imaging*, *IEEE Trans. Nucl. Sci.* **56** (2009) 535.

2013 JINST 8 P07019

[38] C. Szeles et al., *CdZnTe semiconductor detectors for spectroscopic X-ray imaging*, *IEEE Trans. Nucl. Sci.* **55** (2008) 572.

[39] C. Xu et al., *Evaluation of energy loss and charge sharing in cadmium telluride detectors for photon-counting computed tomography*, *IEEE Trans. Nucl. Sci.* **58** (2011) 614.

[40] L. Tlustos, *Spectroscopic X-ray imaging with photon counting pixel detectors*, *Nucl. Instrum. Meth.* **A 623** (2010) 823.

[41] L. Abbene and S. Del Sordo, *CdTe detectors*, in *Comprehensive biomedical physics*, Elsevier, (2013).

2013 JINST 8 P07019